1-9-2018

Unexpected Occurrence of Mesospheric Frontal Gravity Wave Events Over the South Pole (90 degrees S)

P.-D. Pautet
Utah State University

M. J. Taylor
Utah State University

J. B. Snively
Embry-Riddle Aeronautical University, snivelyj@erau.edu

C. Solorio
Utah State University

AGU PUBLICATIONS

JGR

Journal of Geophysical Research: Atmospheres

RESEARCH ARTICLE
10.1002/2017JD027046

Special Section:
Atmospheric Gravity Wave Science in the Polar Regions and First Results from ANGWIN

Unexpected Occurrence of Mesospheric Frontal Gravity Wave Events Over South Pole (90°S)

P.-D. Pautet[1], M. J. Taylor[1], J. B. Snively[2], and C. Solorio[1]

[1]Center for Atmospheric and Space Sciences (CASS), Utah State University, Logan, UT, USA, [2]Department of Physical Sciences and CSAR, Embry-Riddle Aeronautical University, Daytona Beach, FL, USA

Key Points:
- Large number of mesospheric frontal gravity wave events observed over South Pole during four consecutive austral winters
- Their horizontal parameters have been measured and found similar to the general short-period gravity waves population
- The Krassovsky ratios associated with these events seem to indicate that up to 70% are ducted, implying the existence of extensive thermal inversion layers at high latitudes

Correspondence to:
P.-D. Pautet,
dominiquepautet@gmail.com

Citation:
Pautet, P.-D., Taylor, M. J., Snively, J. B., & Solorio, C. (2018). Unexpected occurrence of mesospheric frontal gravity wave events over South Pole (90°S). *Journal of Geophysical Research: Atmospheres*, *123*. https://doi.org/10.1002/2017JD027046

Received 28 APR 2017
Accepted 3 DEC 2017
Accepted article online 12 DEC 2017

Abstract Since 2010, Utah State University has operated an infrared Advanced Mesospheric Temperature Mapper at the Amundsen–Scott South Pole station to investigate the upper atmosphere dynamics and temperature deep within the vortex. A surprising number of "frontal" gravity wave events (86) were recorded in the mesospheric OH(3,1) band intensity and rotational temperature images (typical altitude of ~87 km) during four austral winters (2012–2015). These events are gravity waves (GWs) characterized by a sharp leading wave front followed by a quasi-monochromatic wave train that grows with time. A particular subset of frontal gravity wave events has been identified in the past (Dewan & Picard, 1998) as "bores." These are usually associated with wave ducting within stable mesospheric inversion layers, which allow them to propagate over very large distances. They have been observed on numerous occasions from low-latitude and midlatitude sites, but to date, very few have been reported at high latitudes. This study provides new analyses of the characteristics of frontal events at high latitudes and shows that most of them are likely ducted. The occurrence of these frontal GW events over this isolated region strongly supports the existence of horizontally extensive mesospheric thermal inversion layers over Antarctica, leading to regions of enhanced stability necessary for GW trapping and ducting.

1. Introduction

The mesosphere and lower thermosphere (MLT), located between ~80 and 120 km, connects the lower and middle atmosphere, where most of the gravity wave (GW) sources reside, with the ionosphere–thermosphere system (IT). It defines the IT lower boundary input, which affects the neutral and plasma responses at higher altitudes and thus can directly influence space weather. It is therefore important to understand the MLT structure and dynamics that are deeply affected by the propagation of short period (<1 h) GWs, which alter global circulation and thermal balance when they deposit their momentum and energy (e.g., Fritts & Alexander, 2003, and references cited therein). Short-period GW account for up to 70% of the total momentum transported (Fritts & Vincent, 1987), and their effects include closure of the mesospheric jets, the general circulation from the summer to the winter mesosphere, and the thermal structure of the polar upper atmosphere (Fritts & Alexander, 2003; Holton, 1982). Likewise, the MLT structure also affects the propagation and dissipation of GWs, which are highly dependent on the wind and temperature backgrounds.The nature of a small-scale GW vertical propagation can be characterized by its effective local vertical wavenumber m. In the case of the WKB approximation (where buoyancy frequency varies slowly and gradually), this is frequently obtained through the "refractive index" m^2 of the Taylor–Goldstein equation, here shown in the form derived by Nappo (2002), when the vertical shear (first derivative) and curvature (second derivative) of the horizontal wind are neglected (for a smoothly and gradually varying background wind speed):

$$m^2 = \frac{N^2}{(c-u)^2} - \frac{1}{4H^2} - k^2 \tag{1}$$

where N is the Brunt–Väisälä frequency, c is the wave observed phase speed, u is the background wind in the direction of propagation of the wave, H is the scale height, and k is the wave horizontal wavenumber. The vertical wavenumber strongly depends on two atmospheric parameters: u, the background wind, and T, the background temperature, through N and the scale height H defined by

$$H = \frac{RT}{g} \tag{2}$$

where $R = 287$ J kg^{-1} K^{-1} is the gas constant for the atmosphere below the turbopause and $g = 9.54$ m s^{-2} is the acceleration of gravity. The Brunt–Väisälä frequency N can be expressed as.

$$N = \sqrt{\frac{g}{T}\left(\frac{dT}{dz} + \Gamma\right)} \tag{3}$$

where $\Gamma = 9.5$ K km^{-1} is the adiabatic lapse rate.

In layers where $m^2 > 0$, the wave is able to freely propagate, transporting momentum to a higher/lower altitude (in case of an upward/downward-propagating wave). In layers where m^2 is negative, the wave will be evanescent, and its amplitude will decrease exponentially over altitude. The boundary where $m^2 = 0$ thus indicates the onset of reflection back into the region from where the wave propagated; likewise, possible transmission may occur into another vertically adjacent region where m^2 again becomes >0. When a propagating wave is observed in a region of positive m^2 between two deep layers where m^2 is negative or equal to 0, it will become "ducted" and propagate primarily in the horizontal direction. This may allow for long-distance propagation (e.g., Walterscheid et al., 2000), where vertical leakage from the duct region may occur gradually and over an extended range (Heale, Snively, & Hickey, 2014). These "trapped" or "ducted" waves are a common occurrence at mesospheric altitudes, but their actual percentage, compared to freely propagating or evanescent waves, has not yet been clearly assessed nor quantified. Depending on the study, ducting can vary between ~3% and ~75% of the total number of measured short-period waves (Ejiri et al., 2003; Isler, Taylor, & Fritts, 1997; Nielsen et al., 2012; Walterscheid et al., 1999).

There are two types of gravity wave ducts, each corresponding to a background parameter limiting the wave propagation. "Thermal ducting" occurs when the Brunt–Väisälä frequency N (depending on the vertical temperature, which is defined by the vertical temperature profile) varies with altitude in such a way that it prevents wave propagation (e.g., Bageston et al., 2011; Smith et al., 2005; Walterscheid, Schubert, & Brinkman, 2001). Vertical shear of the horizontal wind u can also create the right conditions for GW reflection and thus affects their propagation and characteristics (e.g., Snively et al., 2007, and references therein); thus, "Doppler ducting" occurs in layers where the wind flow shifts the GW's intrinsic frequency to enable its propagation between layers where the wave becomes evanescent. It should be noted that while thermal ducting is isotropic, Doppler ducting does not affect wave propagation uniformly as it depends on the wind direction (Nault & Sutherland, 2007).

Stable mesospheric thermal structures, where a GW may become ducted, are known as mesospheric inversion layers (MILs) (e.g., Meriwether & Gardner, 2000; Meriwether & Gerrard, 2004). They may appear following GW breaking, when a wave encounters a critical layer (Hauchecorne, Chanin, & Wilson, 1987; Huang et al., 1998) or because of tidal activity (e.g., Fechine et al., 2009; Liu & Hagan, 1998; Meriwether et al., 1998; Walterscheid, 1981; Yuan et al., 2014). They can persist up to several days and extend over large regions ($>$500 km; Smith et al., 2003, 2005). Recent case studies (Bossert et al., 2014; Yuan et al., 2014) have described some of their effects, but MIL reports at high latitudes are rare, especially on the Antarctic continent, because of the lack of observations.

Ducted waves exhibit distinct observable characteristics; they tend to be quasi-monochromatic and coherent especially as they disperse into modes (e.g., Snively & Pasko, 2005, and references therein). Waves with shorter ground-relative periods and higher phase velocities may, in particular, be subject to reflection/ducting at MLT altitudes. They are also more likely to produce in-phase or anti-phase airglow intensity and temperature signatures in airglow (Hines & Tarasick, 1994; Snively, Pasko, & Taylor, 2010).

A particular type of ducted wave observed in the mesosphere is the "bore," which exhibits the primary features discussed above in addition to important evidence of nonlinearity, viz., the presence of steepness and evidence for bulk fluid impacts. Bores on fluid surfaces were first observed in rivers during seasons of incoming tide and initially analyzed by Lord Rayleigh (1908). Large amounts of additional water from the tide overwhelm the outlet of a river, creating an unstable mound of water that eventually breaks into a bore propagating upstream. Bore events would later be observed in the troposphere in the 1970s (e.g., Clarke, Smith, & Reid, 1981; Hartung & Sitkowski, 2010). They were first recorded at mesospheric altitude as "front-like" wave events in the early 1990s, during the Airborne Lidar and Observations of the Hawaiian Airglow 1993 (ALOHA-93) campaign (Taylor, Turnbull, & Lowe, 1995), and it was several years later that Dewan and

Picard (1998) recognized them as such. Since these first reports, many observations of mesospheric bores have been published, mostly at low-latitude (e.g., Fechine et al., 2005, 2009; Narayanan, Gurubaran, & Emperumal, 2009; Shiokawa et al., 2006; Smith et al., 2005, 2006; Walterscheid et al., 2012) or midlatitude sites (e.g., Brown et al., 2004; She et al., 2004; Smith et al., 2003; Yue et al., 2010). Indeed, only one event has been reported from a high-latitude location (Nielsen et al., 2006). This can be explained in part by the shorter record of observations in the polar regions but also by weaker winds in the upper atmosphere at high latitudes, which indicate conditions less favorable for MIL generation, making it more difficult to create Doppler ducts where strongly trapped bores could propagate.

In their subsequent paper, Dewan and Picard (2001) investigated the bore generation mechanisms and their possible origins. They also presented a list of characteristics to identify them. Some of these characteristics should be particularly kept in mind: the phase speed of the front will be ~20–100 m/s; there will be a fixed pattern of trailing crests, with their number gradually increasing over time as the bore dissipates and disperses (in the case of undular bores); there will be a stable layer to provide the duct, formed through some combination of wind shear and/or thermal inversions; and the change in temperature ΔT across the front should be ~$(h_1 - h_0)\Gamma$, with h_0 and h_1 as the undisturbed and disturbed duct depths, respectively, and Γ as the adiabatic lapse rate. If clearly identified, the presence of a bore should confirm that a strong, stable mesospheric duct existed at the time of its observation. Indeed, recent theoretical and modeling efforts have further recognized that mesospheric bores exhibit features consistent with the nonlinear theory for "internal" bores and solitary internal wave trains, which require a stable ducting layer in which waves are generated and subsequently propagate (Laughman, Fritts, & Werne, 2009, 2011; Seyler, 2005).

Another mesospheric phenomenon that appears very similar to bore events in airglow image data (e.g., Smith, 2014) was first described by Swenson and Espy (1995), who proposed the name of "wall" event. It also appears as a sharp bright or dark front followed by trailing crests, but with a phase shift with altitude when observed in several airglow emissions simultaneously. These waves are not clearly ducted but instead propagate freely to higher altitude and thus transport momentum and energy vertically. Differences exist between these two types of waves (i.e., the phase shift over altitude for "wall" events and their absence of ducting), but they will both exhibit very similar characteristics in airglow image data.

This paper will present the unexpected observations of mesospheric frontal events from the South Pole station during four Austral winters (2012–2015) and investigate their characteristics to assess the nature of their propagation. Section 2 will give an overview of the instrumentation and observations. Section 3 will explain the methods used to analyze the image data and to characterize the frontal events. Section 4 will describe their main features and compare them with previous studies of similar phenomena. Section 5 will discuss the possibility that a large fraction of these events may be ducted, revealing important information on the high-latitude mesosphere structure. Finally, conclusions will be given in section 6.

2. Instrumentation–Observations

Airglow imaging of the hydroxyl (OH, ~87 km), sodium (Na, ~90 km), molecular oxygen (O_2, ~92 km), and atomic oxygen green line ($O(^1S)$, ~96 km) emissions has been commonly used for more than 40 years to study the dynamics of the MLT (e.g., Peterson & Kieffaber, 1973; Moreels & Herse, 1977; Swenson & Mende, 1994; Taylor, Bishop, & Taylor, 1995; Nakamura et al., 1999). The first instruments only measured the airglow emission brightness (intensity), but in the 1990s, a new imager was developed at Utah State University (USU) to also map the OH rotational temperature—corresponding to a brightness-weighted temperature—of a large region of the sky. This mesospheric temperature mapper used a back-illuminated CCD detector, a telecentric lens system, and three narrow-band filters to sequentially measure the $P_1(2)$ and $P_1(4)$ lines of the OH(6,2) band, and the sky background intensity at 857 nm. Combining these three emissions, it is possible to calculate the OH(6,2) rotational temperature for each pixel of an image and "map" the mesospheric temperature at ~87 km (Pendleton, Taylor, & Gardner, 2000; Taylor, Gardner, & Pendleton, 2001). This instrument has performed extremely well during the past 20 years (e.g., Taylor et al., 1999; Taori, Taylor, & Franke, 2005; Taori & Taylor, 2006; Zhao, Taylor, & Chu, 2005; Zhao et al., 2007; Simkhada et al., 2009); nevertheless, it is limited to low-latitude and midlatitude observations due to the usual presence of aurora over high-latitude sites. Auroral emissions are brighter than the OH emission in the (6,2) band part of the spectrum and can contaminate the data. Thus, in 2010, a new instrument was developed at USU for high-latitude observations. This

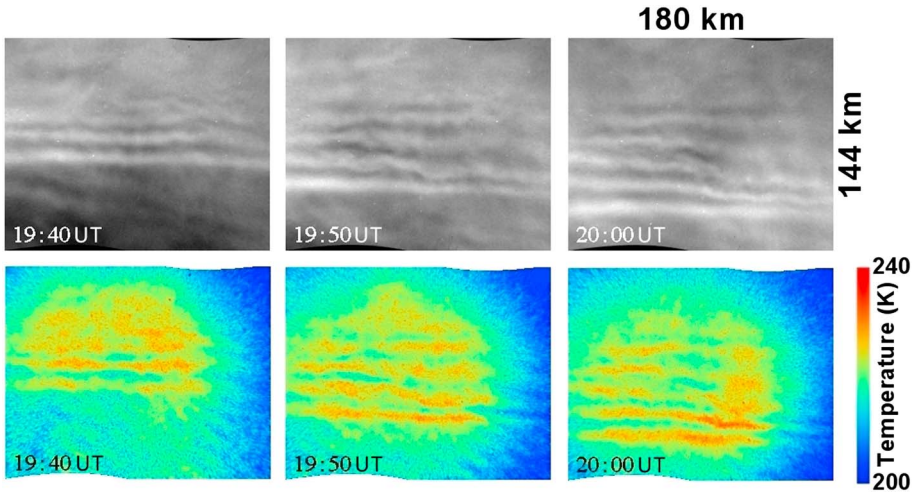

Figure 1. Times series of frontal events observed on 4 May 2013. (top) OH(3,1) band intensity. (bottom) OH(3,1) rotational temperature.

Advanced Mesospheric Temperature Mapper (AMTM) uses a 320 × 256 pixel IR sensor to measure lines of the OH(3,1) band, instead of (6,2), around 1,500 nm. This region of the spectrum is uncontaminated by other emissions under typical nightglow conditions, and auroral emissions are much weaker in this part of the spectrum. Furthermore, the (3,1) band is ~70 times brighter than the (6,2) band and also is less affected by water vapor absorption. Observations in the IR, the angle of view (120°), and the position of the moon, always at low elevation angles at high-latitude sites, enable continuous measurements, even during full-moon conditions. New temperature and band intensity maps are created every ~30 s, revealing the upper atmosphere structure over a ~180 × 144 km region, centered at the zenith. More details about this instrument and its measurements capabilities are given in Pautet et al. (2014).

The first AMTM was deployed in 2010 at the Amundsen–Scott South Pole station to take advantage of the long polar night. It operates 24 h/day during the Austral winter, from mid-April until the end of August, providing an unparalleled data set. During the first two winters of observation (2010 and 2011), the imager operated nominally, but the data were partially obscured by frosting inside the observing dome, limiting our initial studies mainly to long-term temperature evolution, large-scale gravity waves, and tidal features. In 2012, the full potential of the AMTM was reached by continuously purging the dome (sealed to the top lens) with liquid N_2 vapor. Small-scale gravity waves became visible at high spatial resolution, enabling their investigation. In addition, an all-sky airglow imager operated in parallel to the AMTM until Spring 2013. It recorded the OH brightness in the near IR (~900 nm) and was used to provide a larger context to the AMTM observations. This instrument measured weaker lines than the AMTM, but over a larger part of the OH spectrum, thus with a similar sensitivity to GW detection.

Several studies have already revealed the surprisingly large number of mesospheric small-scale GWs propagating over the South Pole, deep inside the polar vortex and without any of the expected GW sources in close proximity (convection, orography, jet stream). Suzuki et al. (2011) described GW characteristics at South Pole using data taken by an all-sky imager between 2003 and 2005 filtered to observe the Na airglow emission. Employing the same data set, Mehta et al. (2016) investigated the possible origin of several events using a ray-tracing technique. The AMTM data similarly show a very high number of small-scale GWs but also provides more information about these waves, including their associated temperature perturbations. Unexpectedly, a large number of these waves exhibited front-like characteristics, usually associated with bore/ducted events: a sharp leading front, followed by a fixed pattern of trailing crests.

During four winter seasons (2012–2015, total 18 months of observations), 86 frontal events were identified (~1 per week), and 68 of those exhibited formation of new trailing crests over time. The other 18 still showed a distinct leading front with several trailing crests, but no more were formed during the time the event was recorded. These 86 events correspond to approximately 10% of all the short-scale GWs observed during the same period. Figure 1 provides a typical example of a South Pole (SP) frontal event shown in both intensity

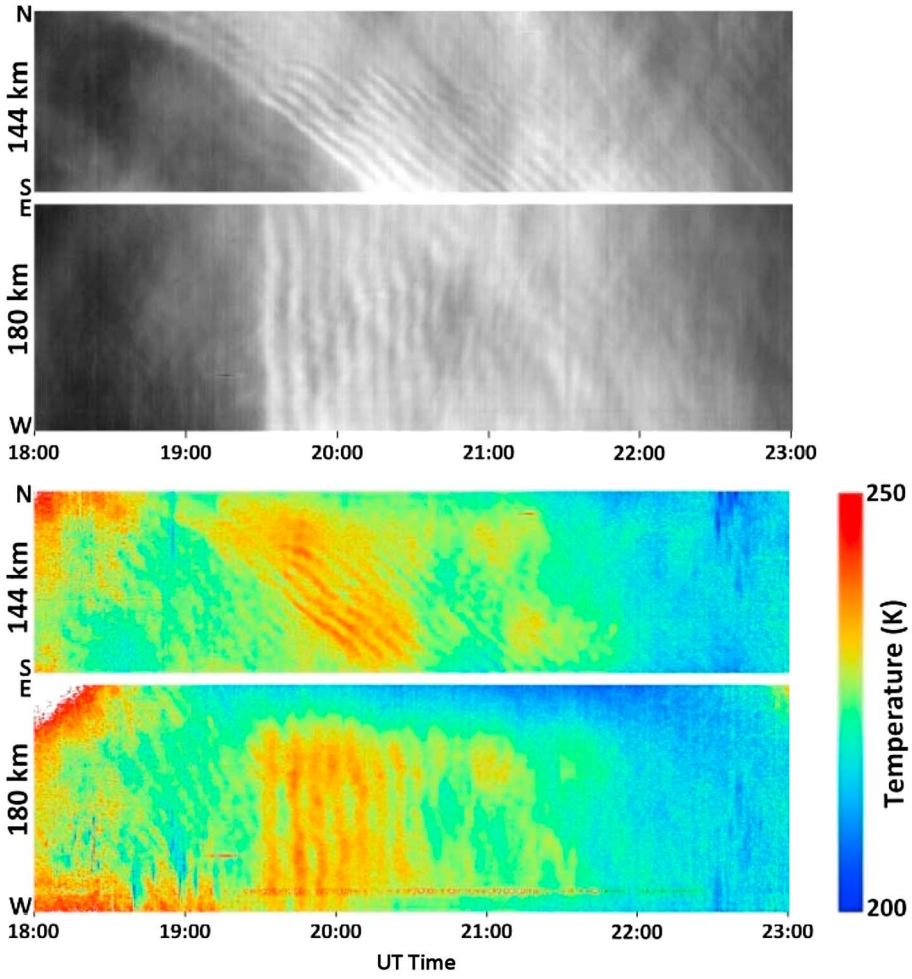

Figure 2. Keogram representations for the frontal event displayed in Figure 1. (top) OH(3,1) band intensity. (bottom) OH(3,1) rotational temperature. Note the large number of trailing waves.

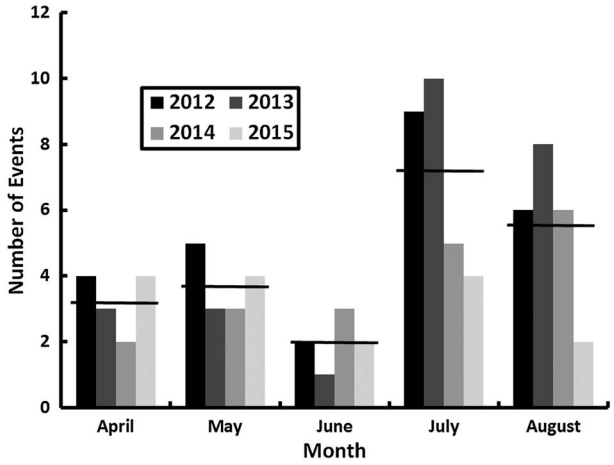

Figure 3. Yearly and monthly fronts distributions (note: the April values correspond to half a month). The horizontal lines correspond to the monthly averages.

(top) and temperature (bottom), which took place on 4 May 2013. The image progression from left to right shows an increase in the number of trailing crests over time. The amount of data obtained each winter season (~3,400 h) makes the search for such events time-consuming, but they can be readily identified within automatically created Keogram images that summarize 24 h periods of observation. As an example, Figure 2 shows the intensity (top) and temperature (bottom) Keograms corresponding to the period when the event in Figure 1 was observed. The sharp leading front and the long series of trailing crests are easily identifiable in both representations. Keograms also give an indication on the main direction of propagation and the number of trailing crests.

The fronts did not occur regularly along the winter as revealed in Figure 3. More events were observed during the months of July and August (7 and 5.5 per month on average, respectively) than before solstice (3.75/month in May and 2/month in June), even if the viewing conditions are usually similar throughout the winter. However, the month of April had a large number of fronts (3.25 in average but for 2 weeks). This result seems consistent for each year, except for August 2015 when only two fronts were observed.

3. Methods and Techniques

After the frontal events have been identified, their characteristics were measured using well-established mathematical tools, such as the fast Fourier transform. Such processing was first described by Coble, Papen, and Gardner (1998) and Garcia, Taylor, and Kelley, (1997) and has since been extensively used in numerous airglow GW studies. The parameters employed to characterize each GW are the horizontal wavelength λ_h, the observed horizontal phase speed c, the observed period τ, the direction of propagation θ, the mean temperature T_0 and intensity I_0, and the temperature and intensity perturbations dT and dI. Two more parameters can also be calculated to characterize frontal events: the number of trailing crests and their generation growth rate. The latter is estimated using the following equation (Dewan & Picard, 1998):

$$\frac{dW}{dt} = \frac{c_i (h_1 - h_0)^3}{2a^2 \lambda_h h_1} \tag{4}$$

Here c_i is the intrinsic horizontal phase speed of the front, λ_h is its horizontal wavelength, h_0 and h_1 are the undisturbed and disturbed duct depths, respectively, and a is the wave amplitude in meters. Note that h_0, h_1, and a can be defined as functions of the other parameters by (Dewan & Picard, 1998; Stockwell et al., 2011)

$$h_1 = \sqrt[3]{\frac{Bc_i^2}{g'} + B\sqrt{\frac{B}{3} + \frac{c_i^4}{g'^2}}} + \sqrt[3]{\frac{Bc_i^2}{g'} - B\sqrt{\frac{B}{3} + \frac{c_i^4}{g'^2}}} \tag{5}$$

$$B = \frac{\lambda_h^2}{2\left(\frac{2\pi}{3}\right)^2} \tag{6}$$

$$h_0 = \frac{g' h_1^2}{2c_i^2 - g' h_1} \tag{7}$$

$$a = \frac{2}{\sqrt{3}}\left(\frac{c_i^2}{g'} - h_1\right) \tag{8}$$

Now g', the buoyant acceleration of gravity, is equal to 1.4 m s^{-2} at 85 km (Dewan & Picard, 1998). Finally, the AMTM allows calculating the Krassovsky ratio associated with each event. This parameter was introduced by Krassovsky (1972), to relate the temperature perturbation induced by GWs to the airglow brightness. It is defined by

$$\eta = \frac{\frac{dI}{I_0}}{\frac{dT}{T_0}} \tag{9}$$

dI and dT are the airglow intensity and brightness-weighted temperature perturbations, respectively, and I_0 and T_0 are the average integrated airglow intensity and brightness-weighted temperature, respectively.

The Krassovsky ratio, η, is a complex quantity and thus can be expressed using its modulus $|\eta|$ and its phase φ; that is, when φ is positive (negative), the intensity leads (lags) the temperature. Following the introduction of the Krassovsky ratio, several theoretical studies investigated the effects of GW propagation on the airglow layers and used it to relate the GW parameters to the airglow response (e.g., Hines & Tarasick, 1987; Schubert, Walterscheid, & Hickey, 1991; Swenson & Gardner, 1998). Subsequently, numerous observations have been compared to these theories using optical measurements, but mostly for long-period (>1 h) GWs or for tides (see Ghodpage et al., 2016, and references therein). Only Reisin and Scheer (2001) have extended the comparison to relatively short-period GWs (~17 min to ~170 min) using measurements of the OH and O_2 emissions made at the zenith by a tilting filter spectrometer from two midlatitude sites: El Leoncito Observatory, Argentina (31.8°S), and El Arenosillo, Spain (37.1°N). The Krassovsky ratio is of relevance for diagnosing ducted waves, since ideal ducting (resonant standing GW structure) is predicted to result in a near-zero or 180° response, depending on chemistry and the layered species profiles (e.g., Hines & Tarasick, 1994; Snively, Pasko, & Taylor, 2010). The SP AMTM measures both the OH(3,1) band intensity and OH(3,1) rotational temperature (height-weighted over the thickness of the OH layer) perturbations associated with a wave (see Figure 1), and consequently, it is possible with this instrument to assess Krassovsky ratios.

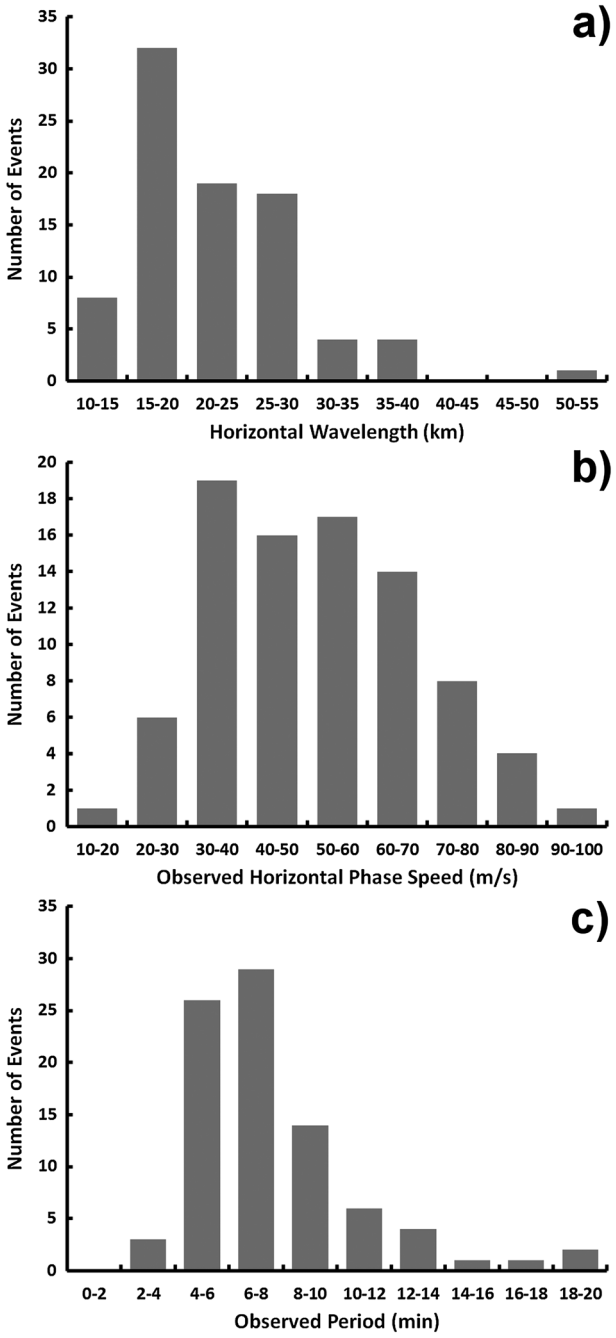

Figure 4. Histograms for the horizontal parameters for 86 frontal events observed from South Pole during four winter seasons (2012–2015). (a) Horizontal wavelength, (b) observed horizontal phase speed, and (c) observed period.

4. Results

Figure 4 illustrates the distributions corresponding to (a) the horizontal wavelengths, (b) the observed horizontal phase speeds, and (c) the observed periods. These distributions are similar to the ones obtained during previous short-period GW studies, in particular, Suzuki et al. (2011), already for the South Pole location. However, the average values were somewhat different: Suzuki et al. measured larger average λ_h (29.2 km for short-period waves compared with 22.0 km for this study) but slightly lower c (49.7 m/s compared with 51.2 m/s), resulting in larger τ (10.3 min compared with 7.8 min). Furthermore, images obtained by the small all-sky OH imager operating in parallel with the AMTM have been analyzed. The winter 2010 short-period GW data show almost identical average values as reported by Suzuki et al. ($\lambda_h = 27.1$ km, $c = 48.7$ m/s, $\tau = 10.1$ min), confirming that the frontal events have similar characteristics as the general short-period GW events, but with shorter average horizontal wavelengths and thus shorter observed periods. These results are also in agreement with other GW studies at lower latitudes (e.g., Medeiros et al., 2003; Nielsen et al., 2009). Additionally, Fechine et al. (2005) investigated frontal events (64, out of a total of 660 short-period GWs over a 2 year period) over São João do Cariri, Brazil (7.5°S), and found similar ranges for the horizontal wavelengths (10–40 km) and the observed phase speeds (10–70 m/s) as the present study.

To completely define the horizontal parameters of GWs, it is normally necessary to know the background wind, u, to calculate the GW intrinsic phase speed, which is equal to $c - u$ and found in equations such as equation (1). Unfortunately, no mesospheric wind data are available after 2011 at the SP; however, earlier measurements can give an estimate of the typical wind values during the winter months. A Fabry–Pérot spectrometer measured the wind at the altitude of the OH layer between 1990 and 2010 (e.g., Hernandez, Smith, & Conner, 1992), and during almost the same period, a meteor radar recorded the mesospheric winds near 95 km altitude (e.g., Portnyagin, Forbes, & Makarov, 1997). Both instruments indicated very weak winds, with normal maximum daily values of $<$20 m/s and unusually short peaks at ~40 m/s. Modeling studies also indicate that mesospheric winds at SP should be weak (Roble, 1992). Therefore, projecting the horizontal wind vectors in the direction of propagation of the GWs should give notably smaller values than typical at midlatitude sites; subsequently, the intrinsic phase speed can be reasonably approximated as being almost equal to the observed phase speed. Indeed, thermal variations may have dominant influence on small-scale propagation in these cases (Snively et al., 2013).

To estimate their possible sources, it is also important to measure the direction of propagation θ of the frontal events. As shown in Figure 5, the fronts exhibit a similar distribution as the complete set of short-period GWs observed from SP. Figure 5a gives the directions of propagation for the frontal events observed during the 2012–2015 winters, while Figure 5b displays the same distribution but for 183 short-period GWs observed during the winter season 2010 by the collocated all-sky OH imager. Both plots show a predominance for wave propagation toward azimuths ~150–330°, corroborating the fact that the frontal events investigated in this study tend to travel in the same direction as typical short-period GWs.

Two other important parameters are shown in Figure 6: (a) the number of trailing crests for each event and (b) the calculated trailing crest growth rates in number of crests per hour. The SP fronts had between 2 and 24

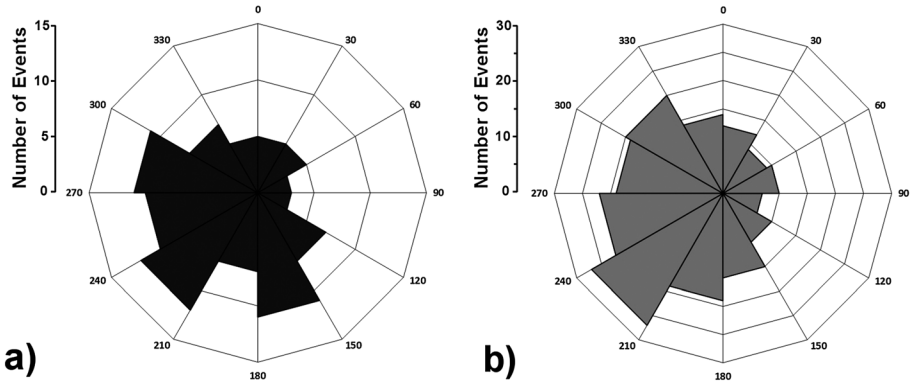

Figure 5. (a) Direction of propagation of 86 frontal events observed during the 2012–2015 winter seasons with the AMTM. (b) Direction of propagation of 183 short-period gravity waves observed during the 2010 winter with the OH all-sky imager.

trailing crests, noticeably more than previously reported. For example, the bore observed at Halley Station, Antarctica, by Nielsen et al. (2006) grew a total of 12 crests, while the extensive bore observed over Texas and described by Smith et al. (2003) had a total of 14 crests. The in-depth study of mesospheric fronts done by Fechine et al. (2005) revealed a range of 2–12 crests, with two to six crests per event being most common. The average number of trailing crests per event over SP is 8.5, with 15 cases (~17%) having more than 12 crests, and a couple observations as much as twice the highest reports in the past. This result implies that those events had already a long lifetime when measured, possibly being ducted over a large distance. It also reveals strong ducting environment, with relatively deep regions of nearly zero stability surrounding the duct (Grimshaw et al., 2015; Laughman, Fritts, & Werne, 2011). It is important to notice that the sensitivity of the AMTM, compared to earlier airglow imagers, could also explain this result, but the all-sky OH camera operating at the SP until 2013, which was similar to the instruments used in previous studies, measured a comparable number of crests on most occasions.

Concerning the trailing crests growth rate, most of the times, observations did not provide precise numbers because the field of view of the AMTM is relatively small. Indeed, on several occasions, it was not possible to see the end of the wave trail and to be sure that no new crests were created. Other times, it was also difficult to determine whether an oscillation appearing close to the edge of the image had just been created or was simply entering the field of view. Nevertheless, it is possible to calculate the theoretical growth rate for the SP events (Dewan & Picard, 1998; Stockwell et al., 2011). As shown in Figure 6b, the average number is 0.95 crests/h, with 67% of the values between 0.5 and 1.5 crests/h. This result is similar to, but somewhat smaller than, previous studies; the theoretical estimate by Dewan and Picard (1998) for the Taylor, Turnbull, and Lowe, (1995) event was 2.8 crests/h, Smith et al. (2003) measured a value of 1.0 ± 0.8 crests/h, and Smith et al. (2005), for another event observed over Puerto Rico, obtained values of 3.0 crests/h from measurements and 1.9 crests/h from theory. More recently, Li et al. (2013) computed a maximum rate of 2.43 crests/h for a bore recorded over northern China, and Narayanan, Gurubaran, and Emperumal (2009) calculated a value of 3.6 crests/h for another

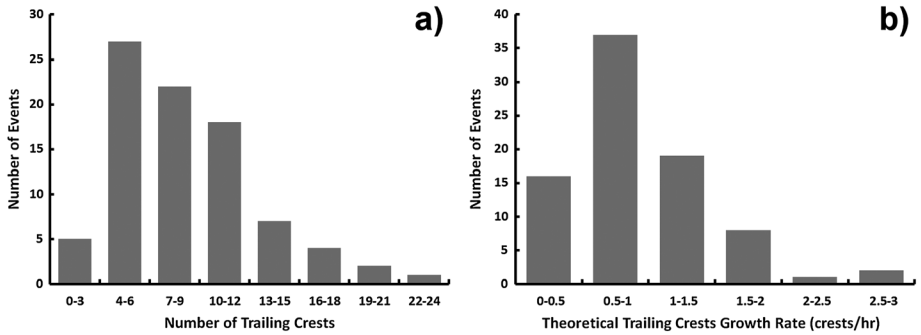

Figure 6. (a) Number of trailing crests associated with the SP fronts. (b) Theoretical generation rate for the same events.

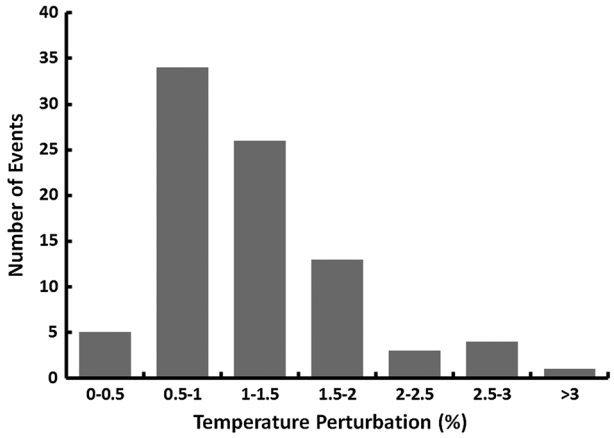

Figure 7. Temperature perturbations for the 86 SP fronts.

bore event over southern India. The range of values calculated for the SP events is in good agreement with these previous results.

The next parameter of interest is the temperature perturbations d*T* created by the wave events. It can only be measured by instruments like the AMTM, which provide not only the airglow brightness but also the OH rotational temperature. The values are obtained using an FFT analysis method and correspond to the average perturbation over the front and its trailing crests. Figure 7 shows the distribution for the 86 events. The average value is 1.2% with 85% of the values between 0.5% and 2.0%. Intensity d*I* perturbations have also been measured using the same method.

5. Discussion

The fronts observed in the MLT over the SP during the 2012–2015 winters exhibit several characteristics similar to those of bore events as defined by Dewan and Picard (2001). This type of GWs has been described in numerous studies but almost exclusively from low-latitude or midlatitude sites. They are a good indicator of wave ducting enabled by the presence of a stable layer, due to a temperature inversion (MIL), or a sheared wind profile due to large-scale wave motions. However, it is normally difficult to confirm that such stable ducts exist without additional measurements of temperature profiles, as obtained by lidars, to identify inversion layers (and define *N*), or wind profiles from meteor radars, to estimate Doppler shifts and wind shear effects. None of these instruments were operating at the SP when the AMTM was taking the data, so there is no direct way to positively confirm the presence of MILs or Doppler ducts. Nevertheless, the confirmation that some of the extensive frontal events were consistent with bores or ducted waves strongly supports the possibility that they propagated within a stable ducting environment, such as likely provided by an MIL.

Figure 8 shows an example of temperature and intensity horizontal profiles recorded perpendicularly to the wave front of the Figure 1 event. The data have been demeaned, detrended, and smoothed. The phase shift φ is then measured by calculating the cross-correlation coefficient between the two curves. In this case, both profiles were almost perfectly in phase, with $\varphi = 0.1° \pm 10°$. The 86 SP events have been processed in the same way and their Krassovsky ratio calculated, as shown in Figure 9. The modulus (Figure 9a) has an average value of 5.5 ± 0.2 (minimum 1.7, maximum 11.1) for observed periods between ~4 and ~20 min. This value is larger than previous measurements: Reisin and Scheer (2001) obtained $|\eta| = 1.68 \pm 0.07$ for the OH emission as well, and periods between 17 and 170 min, while other measurements for GWs with periods over 2 h and tides resulted in values between ~2 and ~10, but with usually smaller numbers for shorter periods. Such a large range of values appears in all studies. Indeed, Hines and Tarasick (1987) noted that a strong dependence exists between the GW parameters and both the intensity and temperature perturbations, resulting in a complicated relation for $|\eta|$. Figure 10 shows the distribution of $|\eta|$ as a function of the fronts' observed periods. No straightforward correlation appears, as in previous investigations. Similar plots (not shown) do not exhibit any direct relationship as well between the Krassovsky ratio and other wave parameters (horizontal wavelength and observed horizontal phase speed). Snively, Pasko, and Taylor (2010) also found that the Krassovsky ratio was determined primarily by the vertical structure of the gravity waves as they perturbed the airglow species and was strongly dependent on the altitude of the duct relative to the layer and thus also the shape of the layer.

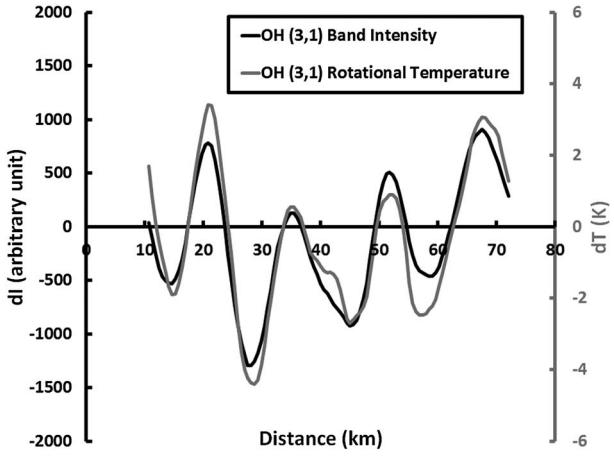

Figure 8. Intensity and temperature profiles measured across the 4 May 2013 frontal event.

However, the Krassovsky ratio phase φ provides more relevant information on the waves, in particular, about the possibility that they experienced strong ducting. For the SP events (Figure 9b), the average value was $-12.2° \pm 3°$, with 31% of the phases $>0°$, implying a downward phase propagation, as explained by several models (Hines &

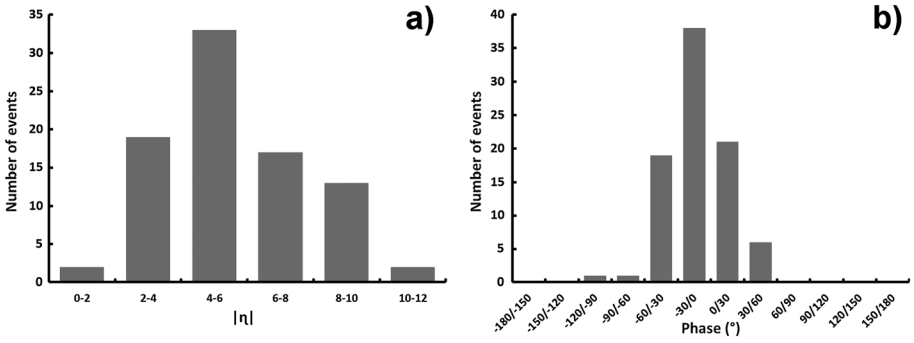

Figure 9. (a) Krassovsky ratio modulus and (b) phase for the 86 SP frontal events.

Tarasick, 1987; Swenson & Gardner, 1998). Reisin and Scheer (2001) found somewhat similar values ($-17° \pm 2°$, 39% of positive phases) but with a much wider distribution: only 28% of their GWs had $|\varphi| < 30°$, while 69% of the SP fronts were in that case. In other studies involving long-period GWs and tides, $|\varphi|$ was almost exclusively $>25°$ (Ghodpage et al., 2016). In theory, a zero-phase shift corresponds to vertically evanescent GWs, or GWs with a very large vertical wavelength (>200 km), but Hines and Tarasick (1994) have explained that it can also result from a wave being reflected or trapped into a duct, because of the vertical cancellation of phase shift in the integrated signatures (Snively & Pasko, 2005). In fact, the phase does not have to be exactly 0°; several processes can slightly modify φ, especially if the wave is not perfectly resonant within the duct, if the photochemistry involves time scales comparable to the wave period, or if the observations are off-zenith (Hines & Tarasick, 1994; Snively, Pasko, & Taylor, 2010). Nonetheless, small phase shifts seem generally associated with ducted or evanescent waves with large vertical wavelengths. The large proportion of possibly ducted fronts (~70%) implies that stable layers and, most likely, mesospheric inversion layers do indeed occur over the wintertime South Polar Region. This study only discusses a specific type of waves, which are just a small part of the full short-period GW spectrum but are easy to identify and analyze. Nonfrontal events can also be ducted: any monochromatic, fast, long lasting GW might be trapped. Nevertheless, a main result of this analysis is that MILs commonly exist at high latitudes, even with small horizontal winds, and have to be accounted for to determine the origin of observed GWs.

Other investigations have tentatively studied the nature of these short-period waves from high-latitude locations. Suzuki et al. (2011) used meteor radar wind data in association with their Na all-sky images to estimate m^2. They found that ~10% of their GWs were evanescent. Unfortunately, they only had wind measurements height-weighted around 92 km and no vertical temperature profiles. Similarly, Suzuki et al. (2009), using the same type of instruments, investigated the propagation of GWs over Resolute Bay, Canada (75°N), and found ~13% of evanescent waves, but again without assessing the atmospheric vertical structure. Nielsen et al. (2012) investigated further the data set introduced by Nielsen et al. (2009) who presented the climatology of short-period GWs over Halley (76°S) using OH all-sky images and meteor radar wind measurements. This time, they also utilized collocated SABER temperature data and discovered that while Doppler ducting was rare at this latitude (~5% of the waves), 28% of their temperature profiles featured a thermal duct (while 54% showed freely propagating conditions throughout the MLT region, and 18% suggested evanescence). Snively et al. (2013) subsequently modeled the atmospheric conditions over Halley to investigate the parameter space of the GWs identified by Nielsen et al. (2009). They concluded that up to 70% of these waves might have experienced some form of thermal reflection, evanescence, or ducting at some altitude(s) within the atmosphere, 25% of them in the lower thermosphere region. Further simulations by Heale, Snively, and Hickey (2014) also support the results of Snively et al. (2013) and identify some role for the weak wind flow

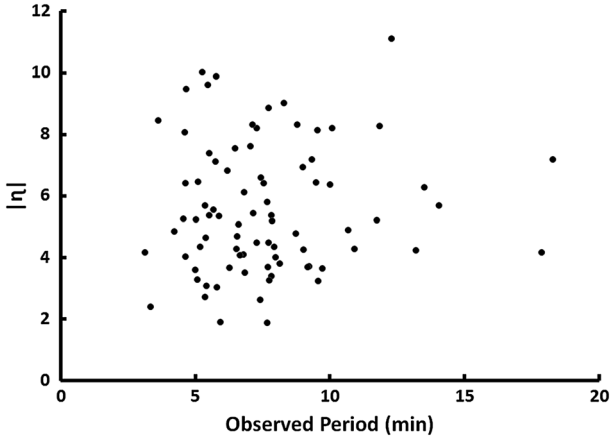

Figure 10. Krassovsky ratio modulus as a function of the SP frontal events observed period.

and, additionally, find a role for the stratosphere to enable ducting over long distances, where waves may leak upward into the mesosphere and lower thermosphere (where they may also be ducted).

The frequent occurrence of short-period GWs observed over the South Pole station and other remote high-latitude sites is an unexpected result, since typical GW sources (convection or orography) are absent, except around the Antarctic Peninsula (Hoffmann, Xue, & Alexander, 2013). Other GW sources such as unbalance flow of the Polar Night Jet or secondary GW generation in the stratosphere or lower mesosphere (Chen et al., 2013, 2016) could potentially be the origin of some of the SP GWs. Nevertheless, the structure of the atmosphere itself may also provide some explanation for this result, suggesting the existence of wave ducting within mesospheric inversion layers and allowing for GW propagation over long distances (e.g., Heale, Snively, & Hickey, 2014; Pautet et al., 2005). The surprisingly large number of frontal events over South Pole, with characteristics similar to ducted waves (short ground-relative periods, high horizontal phase speeds, large numbers of quasi-monochromatic trailing crests that may increase with time, and in-phase temperature and intensity perturbations), suggests that thermal ducting (since the small mesospheric winds at the South Pole latitude generally prevent the generation of Doppler ducts) may indeed play a significant role in GW propagation at high latitudes (France et al., 2015).

6. Conclusion

Since 2010, an Advanced Mesospheric Temperature Mapper has measured the OH(3,1) band intensity and rotational temperature from mid-April to end of August at the South Pole station. Examination of data taken during four consecutive austral winters (2012–15) reveals an unexpected number of front-like GWs. The 86 events exhibited characteristics similar to bores, indicative of the presence of mesospheric inversion layers, but the current lack of supporting data on the prevailing background wind and temperature field limits our ability to establish their propagation, ducting, and sources. Taking full advantage of the capabilities of the AMTM, it was nevertheless possible to obtain more information about these frontal wave events and the atmospheric background. Some important findings are as follows:

1. Frontal events are not rare at high latitudes (~1 per week during winter).
2. Their characteristics are similar to the general short-period gravity waves population, and they travel in the same typical direction.
3. However, their horizontal wavelengths are in average shorter, and consequently, their periods are shorter as well.
4. The Krassovsky ratio phases associated with these events indicate that possibly ~70% are ducted and therefore might be bores.
5. In this case, the large number of their trailing waves (more than in any previous observations) suggests that a significant proportion of events may have been ducted over very long trans-Antarctic distances up to $>$1,000 km.
6. Thus, this reveals the presence of extensive thermal ducts at high latitudes.

This study provides insight on the atmospheric dynamics deep inside the winter polar vortex and gives more evidence for GW long-range ducting, likely by thermal structure, which could explain why so many short-period GWs are observed at high latitudes, especially over the Antarctic Continent, far from typical sources. More AMTM observations with a collocated lidar would be most beneficial to confirm the existence of mesospheric inversion layers. Such a facility now exists at McMurdo station (78°S) and hopefully will further improve our knowledge on the high-latitude upper atmosphere structure and its effects on GW propagation.

Acknowledgments
The authors would like to thank the USAP personnel at the Amundsen–Scott South Pole station for their help in maintaining and operating the AMTM instrument, especially the winter over Research Assistants: John Maloney, Sue O'Reilly, Andrew Vernaza, Neal Scheibe, Hans Boenish, and Tim Ager. The South Pole AMTM was developed and operated under the NSF OPP grants 0542164, 1045356, and 1143587. J. B. Snively acknowledges support under NSF 1151746 to ERAU. The complete South Pole image data sets are available through the USU Box (http://digital-commons.usu.edu/ail/). Password to access the database can be provided upon request to the authors.

References

Bageston, J. V., Wrasse, C. M., Hibbins, R. E., Batista, P. P., Gobbi, D., Takahashi, H., … Denardini, C. M. (2011). Case study of a mesospheric wall event over Ferraz station, Antarctica (62°S). *Annales de Geophysique*, *29*, 209–219.

Bossert, K., Fritts, D. C., Pautet, P.-D., Taylor, M. J., Williams, B. P., & Pendleton, W. R. Jr. (2014). Investigation of a mesospheric gravity wave ducting event using coordinated sodium lidar and mesospheric mapper measurements at ALOMAR, Norway (69°N). *Journal of Geophysical Research: Atmospheres*, *199*, 9765–9778. https://doi.org/10.1002/2014JD021460

Brown, L. B., Gerrard, A. J., Meriwether, J. W., & Makela, J. J. (2004). All-sky imaging observations of mesospheric fronts in OI 557.7 nm and broadband OH emissions: Analysis of frontal structure, atmospheric background conditions, and potential sourcing mechanisms. *Journal of Geophysical Research*, *109*, D19104. https://doi.org/10.1029/2003JD004223

Chen, C., Chu, X., McDonald, A. J., Vadas, S. L., Yu, Z., Fong, W., & Lu, X. (2013). Inertia–gravity waves in Antarctica: A case study using simultaneous lidar and radar measurements at McMurdo/Scott Base (77.8°S, 166.7°E). *Journal of Geophysical Research: Atmospheres*, *118*, 2794–2808. https://doi.org/10.1002/jgrd.50318

Chen, C., Chu, X., Zhao, J., Roberts, B. R., Yu, Z., Fong, W., … Smith, J. A. (2016). Lidar observations of persistent gravity waves with periods of 3–10 h in the Antarctic middle and upper atmosphere at McMurdo (77.83°S, 166.67°E). *Journal of Geophysical Research: Space Physics*, *121*, 1483–1502. https://doi.org/10.1002/2015JA022127

Clarke, R. H., Smith, R. K., & Reid, D. G. (1981). The morning glory of the Gulf of Carpentaria: An atmospheric undular bore. *Monthly Weather Review*, *109*, 1726–1750.

Coble, M. R., Papen, G. C., & Gardner, C. S. (1998). Computing two-dimensional unambiguous horizontal wavenumber spectra from OH airglow images. *IEEE Transactions on Geoscience and Remote Sensing*, *36*, 2.

Dewan, E. M., & Picard, R. H. (1998). Mesospheric bores. *Journal of Geophysical Research*, *103*, 6295–6305.

Dewan, E. M., & Picard, R. H. (2001). On the origin of mesospheric bores. *Journal of Geophysical Research*, *106*(3), 2921–2927. https://doi.org/10.1029/2000JD900697

Ejiri, M. K., Shiokawa, K., Ogawa, T., Igarashi, K., Nakamura, T., & Tsuda, T. (2003). Statistical study of short-period gravity waves in OH and OI nightglow images at two separated sites. *Journal of Geophysical Research*, *108*(D21), 4679. https://doi.org/10.1029/2002JD002795

Fechine, J., Medeiros, A. F., Buriti, R. A., Takahashi, H., & Gobbi, D. (2005). Mesospheric bore events in the equatorial middle atmosphere. *Journal of Atmospheric and Solar: Terrestrial Physics*, *67*, 1774–1778.

Fechine, J., Wrasse, C. M., Takahashi, H., Medeiros, A. F., Batista, P. P., Clemesha, B. R., … Russell, J. M. (2009). First observation of an undular mesospheric bore in a Doppler duct. *Annales de Geophysique*, *27*, 1399–1406.

France, J. A., Harvey, V. L., Randall, C. E., Collins, R. L., Smith, A. K., Peck, E. D., & Fang, X. (2015). A climatology of planetary wave-driven mesospheric inversion layers in the extratropical winter. *Journal of Geophysical Research: Atmospheres*, *120*, 399–413. https://doi.org/10.1002/2014JD022244

Fritts, D. C., & Alexander, M. J. (2003). Gravity wave dynamics and effects in the middle atmosphere. *Reviews of Geophysics*, *41*, 1003. https://doi.org/10.1029/2001RG000106

Fritts, D. C., & Vincent, R. A. (1987). Mesospheric momentum flux studies at Adelaide, Australia: Observations and a gravity wave/tidal interaction model. *Journal of the Atmospheric Sciences*, *44*, 605–848.

Garcia, F., Taylor, M. J., & Kelley, M. (1997). Two-dimensional spectral analysis of mesospheric airglow image data. *Applied Optics*, *36*, 7374–7385.

Ghodpage, R. N., Hickey, M. P., Taori, A. K., Siingh, D., & Patil, P. T. (2016). Response of OH airglow emissions to mesospheric gravity waves and comparisons with full-wave model simulation at a low-latitude Indian station. *Atmospheric Chemistry and Physics*, *16*, 5611–5621.

Grimshaw, R., Broutman, D., Laughman, B., & Eckermann, S. D. (2015). Solitary waves and undular bores in a mesosphere duct. *Journal of the Atmospheric Sciences*, *72*(11), 4412–4442.

Hartung, D. C., & Sitkowski, M. (2010). An atmospheric undular bore along the eastern Florida coast. *Weather*, *65*, 148–150. https://doi.org/10.1002/wea.538

Hauchecorne, A., Chanin, M. L., & Wilson, R. (1987). Mesospheric temperature inversion and gravity wave breaking. *Geophysical Research Letters*, *14*, 933–936.

Heale, C. J., Snively, J. B., & Hickey, M. P. (2014). Numerical simulation of the long-range propagation of gravity wave packets over Halley, Antarctica. *Journal of Geophysical Research: Atmospheres*, *119*, 11,116–11,134. https://doi.org/10.1002/2014JD022099

Hernandez, G., Smith, R. W., & Conner, J. F. (1992). Neutral wind and temperature in the upper mesosphere above South Pole, Antarctica. *Geophysical Research Letters*, *19*(1), 53–56.

Hines, C. O., & Tarasick, D. W. (1987). On the detection and utilization of gravity waves in airglow studies. *Planetary and Space Science*, *35*, 851–866.

Hines, C. O., & Tarasick, D. W. (1994). Airglow response to vertically standing gravity waves. *Geophysical Research Letters*, *21*, 2729–2732.

Hoffmann, L., Xue, X., & Alexander, M. J. (2013). A global view of stratospheric gravity wave hotspots located with Atmospheric Infrared Sounder observations. *Journal of Geophysical Research: Atmospheres*, *118*, 416–434. https://doi.org/10.1029/2012JD018658

Holton, J. R. (1982). The role of gravity wave induced drag and diffusion in the momentum budget of the mesosphere. *Journal of the Atmospheric Sciences*, *39*, 791–799.

Huang, T. Y., Hur, H., Tuan, T. F., Li, X., Dewan, E. M., & Picard, R. H. (1998). Sudden narrow temperature-inversion-layer formation in ALOHA-93 as a critical-layer-interaction phenomenon. *Journal of Geophysical Research*, *103*, 6323–6332.

Isler, J. R., Taylor, M. J., & Fritts, D. C. (1997). Observational evidence of wave ducting and evanescence in the mesosphere. *Journal of Geophysical Research*, *102*, 26,301–26,313.

Krassovsky, V. I. (1972). Infrasonic variations of the OH emission in the upper atmosphere. *Annals of Geophysics*, *28*, 739–746.

Laughman, B., Fritts, D. C., & Werne, J. (2009). Numerical simulation of bore generation and morphology in thermal and Doppler ducts. *Annales de Geophysique*, *27*, 511–523.

Laughman, B., Fritts, D. C., & Werne, J. (2011). Comparisons of predicted bore evolutions by the Benjamin–Davis–Ono and Navier–Stokes equations for idealized mesopause thermal ducts. *Journal of Geophysical Research*, *116*, D02010. https://doi.org/10.1029/2010JD014409

Li, Q., Xu, J., Yue, J., Liu, X., Yuan, W., Ning, B., … Younger, J. P. (2013). Investigation of a mesospheric bore event over northern China. *Annales de Geophysique*, *31*, 409–418. https://doi.org/10.5194/angeo-31-409-2013

Liu, H.-L., & Hagan, M. E. (1998). Local heating/cooling of the mesosphere due to gravity wave and tidal coupling. *Geophysical Research Letters*, *25*, 941–944.

Medeiros, A. F., Taylor, M. J., Takahashi, H., Batista, P. P., & Gobbi, D. (2003). An investigation of gravity wave activity in the low-latitude upper mesosphere: Propagation direction and wind filtering. *Journal of Geophysical Research*, *108*(D14), 4411. https://doi.org/10.1029/2002JD002593

Mehta, D., Gerrard, A. J., Ebihara, Y., Weatherwax, A. T., & Lanzerotti, L. J. (2016). Short-period mesospheric gravity waves and their sources at the South Pole. *Atmospheric Chemistry and Physics Discussions*, *17*, 911–919. https://doi.org/10.5194/acp-17-911-2017

Meriwether, J. W., & Gardner, C. S. (2000). A review of the mesosphere inversion layer phenomenon. *Journal of Geophysical Research*, *105*, 12,405–12,416.

Meriwether, J. W., & Gerrard, A. J. (2004). Mesosphere inversion layers and stratosphere temperature enhancements. *Reviews of Geophysics*, *42*, RG3003. https://doi.org/10.1029/2003RG000133

Meriwether, J. W., Gao, X., Wickwar, V. B., Wilkerson, T., Beissner, K., Collins, S., & Hagan, M. E. (1998). Observed coupling of the mesosphere inversion layer to the thermal tidal structure. *Geophysical Research Letters*, *25*, 1479–1482. https://doi.org/10.1029/98GL00756

Moreels, G., & Herse, M. (1977). Photographic evidence of waves around the 85 km-level. *Planetary and Space Science*, *25*, 265.
Nakamura, T., Higashikawa, A., Tsuda, T., & Matsushita, Y. (1999). Seasonal variations of gravity wave structures in OH airglow with a CCD imager at Shigaraki. *Earth, Planets and Space*, *51*, 897.
Nappo, C. J. (2002). *Atmospheric gravity waves*, *International Geophysical Services* (Vol. 85). San Diego, CA: Academic.
Narayanan, V. L., Gurubaran, S., & Emperumal, K. (2009). A case study of a mesospheric bore event observed with an all-sky airglow imager at Tirunelveli (8.7°N). *Journal of Geophysical Research*, *114*, D08114. https://doi.org/10.1029/2008JD010602
Nault, J. T., & Sutherland, B. R. (2007). Internal wave tunneling across a mixed region. *Physics of Fluids*, *19*, 016601.
Nielsen, K., Taylor, M. J., Stockwell, R. G., & Jarvis, M. J. (2006). An unusual mesospheric bore event observed at high latitudes over Antarctica. *Geophysical Research Letters*, *33*, L07803. https://doi.org/10.1029/2005GL025649
Nielsen, K., Taylor, M. J., Hibbins, R. E., & Jarvis, M. J. (2009). Climatology of short-period mesospheric gravity waves over Halley, Antarctica (76°S, 27°W). *Journal of Atmospheric and Solar: Terrestrial Physics*, *71*, 991–1000.
Nielsen, K., Taylor, M. J., Hibbins, R., Jarvis, M., & Russell, J. (2012). On the nature of short-period mesospheric gravity wave propagation over Halley, Antarctica. *Journal of Geophysical Research*, *117*, D05124. https://doi.org/10.1029/2011JD016261
Pautet, P.-D., Taylor, M. J., Liu, A. Z., & Swenson, G. R. (2005). Climatology of short-period gravity waves observed over northern Australia during the Darwin Area Wave Experiment (DAWEX) and their dominant source regions. *Journal of Geophysical Research*, *110*, D03S90. https://doi.org/10.1029/2004JD004954
Pautet, P.-D., Taylor, M. J., Pendleton, W. R. Jr., Zhao, Y., Yuan, T., Esplin, R., & McLain, D. (2014). An Advanced Mesospheric Temperature Mapper for high-latitude airglow studies. *Applied Optics*, *53*(26), 5934–5943.
Pendleton, W. R. Jr., Taylor, M. J., & Gardner, L. C. (2000). Terdiurnal oscillations in OH Meinel rotational temperatures for fall conditions at northern midlatitude sites. *Geophysical Research Letters*, *27*(12), 1799–1802.
Peterson, A. W., & Kieffaber, L. M. (1973). Infrared photography of OH airglow structures. *Nature*, 24492, 92.
Portnyagin, Y. I., Forbes, J. M., & Makarov, N. A. (1997). Unusual characteristics of lower thermosphere prevailing winds at South Pole. *Geophysical Research Letters*, *24*(1), 81–84.
Rayleigh, L. (1908). Note on tidal bores. *Proceedings of the Royal Society of London*, *81*, 448–449. https://doi.org/10.1098/rspa.1908.0102
Reisin, E. R., & Scheer, J. (2001). Vertical propagation of gravity waves determined from zenith observations of airglow. *Advances in Space Research*, *27*(10), 1743–1748.
Roble, R. G. (1992). The polar lower thermosphere. *Planetary and Space Science*, *40*(I/3), 271497.
Schubert, G., Walterscheid, R. L., & Hickey, M. P. (1991). Gravity wave-driven fluctuations in OH nightglow from an extended, dissipative emission region. *Journal of Geophysical Research*, *96*, 13,869–13,880.
Seyler, C. E. (2005). Internal waves and undular bores in mesospheric inversion layers. *Journal of Geophysical Research*, *110*, D09S05. https://doi.org/10.1029/2004JD004685
She, C. Y., Li, T., Williams, B. P., Yuan, T., & Picard, R. H. (2004). Concurrent OH imager and sodium temperature/wind lidar observations of a mesopause undular bore event over Fort Collins/Platteville, CO. *Journal of Geophysical Research*, *109*, D22107. https://doi.org/10.1029/2004JD004742
Shiokawa, K., Suzuki, S., Otsuka, Y., Ogawa, T., Nakamura, T., Mlynczak, M., & Russell, J. M. (2006). A multi-instrument measurement of a mesospheric front-like structure at the equator. *Journal of the Meteorological Society of Japan*, *84A*, 305–316.
Simkhada, D. B., Snively, J. B., Taylor, M. J., & Franke, S. J. (2009). Analysis and modeling of ducted and evanescent gravity waves observed in the Hawaiian airglow. *Annales de Geophysique*, *27*, 3213–3224.
Smith, S. M. (2014). The identification of mesospheric frontal gravity-wave events at a mid-latitude site. *Advances in Space Research*, *54*, 417–424.
Smith, S. M., Taylor, M. J., Swenson, G. R., She, C. Y., Hocking, W., Baumgardner, J., & Mendillo, M. (2003). A multi-diagnostic investigation of the mesospheric bore phenomenon. *Journal of Geophysical Research*, *108*, 1083. https://doi.org/10.1029/2002JA009500
Smith, S. M., Friedman, J., Rashida, S., Tepley, C., Baumgardner, J., & Mendillo, M. (2005). Evidence of mesospheric bore formation from a breaking gravity wave event: simultaneous imaging and lidar measurements. *Journal of Atmospheric and Solar: Terrestrial Physics*, *67*, 345–356. https://doi.org/10.1016/j.jastp.2004.11.008
Smith, S. M., Scheer, J., Reisin, E., Baumgardner, J., & Mendillo, M. (2006). Characterization of two exceptionally strong mesospheric wave events observed at El Leoncito, Argentina, using all-sky and zenith airglow observations. *Journal of Geophysical Research*, *111*, A09309. https://doi.org/10.1029/2005JA011197
Snively, J. B., & Pasko, V. P. (2005). Antiphase OH and OI airglow emissions induced by a short-period ducted gravity wave. *Geophysical Research Letters*, *32*, L08808. https://doi.org/10.1029/2004GL022221
Snively, J. B., Pasko, V. P., Taylor, M. J., & Hocking, W. K. (2007). Doppler ducting of short-period gravity waves by midlatitude tidal wind structure. *Journal of Geophysical Research*, *112*, A03304. https://doi.org/10.1029/2006JA011895
Snively, J. B., Pasko, V. P., & Taylor, M. J. (2010). OH and OI airglow layer modulation by ducted short-period gravity waves: Effects of trapping altitude. *Journal of Geophysical Research*, *115*, A11311. https://doi.org/10.1029/2009JA015236
Snively, J. B., Nielsen, K., Hickey, M. P., Heale, C. J., Taylor, M. J., & Moffat-Griffin, T. (2013). Numerical and statistical evidence for long-range ducted gravity wave propagation over Halley, Antarctica. *Geophysical Research Letters*, *40*, 1–5. https://doi.org/10.1002/grl.50926
Stockwell, R. G., Taylor, M. J., Nielsen, K., & Jarvis, M. J. (2011). The evolution of a breaking mesospheric bore wave packet. *Journal of Geophysical Research*, *116*, D19102. https://doi.org/10.1029/2010JD015321
Suzuki, S., Shiokawa, K., Hosokawa, K., Nakamura, K., & Hocking, W. K. (2009). Statistical characteristics of polar cap mesospheric gravity waves observed by an all-sky airglow imager at Resolute Bay, Canada. *Journal of Geophysical Research*, *114*, A01311. https://doi.org/10.1029/2008JA013652
Suzuki, S., Tsutsumi, M., Palo, S., Ebihara, Y., Taguchi, M., & Ejiri, M. (2011). Short-period gravity waves and ripples in the South Pole mesosphere. *Journal of Geophysical Research*, *116*, D19109. https://doi.org/10.1029/2011JD015882
Swenson, G. R., & Espy, P. J. (1995). Observations of 2-dimensional airglow structure and Na density from the ALOHA, October 9, 1993 'storm flight'. *Geophysical Research Letters*, *22*, 2845–2848.
Swenson, G. R., & Gardner, C. S. (1998). Analytical models for the response of the mesospheric OH* and Na layers to atmospheric gravity waves. *Journal of Geophysical Research*, *103*(D6), 6271–6294.
Swenson, G. R., & Mende, S. B. (1994). OH emissions and gravity waves (including a breaking wave) in all-sky imagery from Bear Lake, Utah. *Geophysical Research Letters*, *21*, 2239.
Taori, A., & Taylor, M. J. (2006). Characteristics of wave induced oscillations in the mesospheric O_2 emission intensity and temperature. *Geophysical Research Letters*, *33*, L01813. https://doi.org/10.1029/2005GL024442
Taori, A., Taylor, M. J., & Franke, S. (2005). Terdiurnal wave signatures in the upper mesospheric temperature and their association with the wind field at low latitudes (20°N). *Journal of Geophysical Research*, *110*, D09S06. https://doi.org/10.1029/2004JD004564

Taylor, M. J., Bishop, M. B., & Taylor, V. (1995). All-sky measurements of short period waves imaged in the OI (557.7 nm), Na (589.2 nm) and near infrared OH and O_2 (0,1) nightglow emissions during the ALOHA-93 campaign. *Geophysical Research Letters*, *22*, 2833.

Taylor, M. J., Turnbull, D. N., & Lowe, R. P. (1995). Spectrometric and imaging measurements of a spectacular gravity wave event observed during the ALOHA-93 campaign. *Geophysical Research Letters*, *22*, 2849–2852.

Taylor, M. J., Pendleton, W. R. Jr., Gardner, C. S., & States, R. J. (1999). Comparison of terdiurnal tidal oscillations in mesospheric OH rotational temperature and Na lidar temperature measurements at mid latitudes for fall/spring conditions. *Earth, Planets and Space*, *51*, 877–885.

Taylor, M. J., Gardner, L. C., & Pendleton, W. R. Jr. (2001). Long period wave signatures in mesospheric OH Meinel (6,2) band intensity and rotational temperature at mid latitudes. *Advances in Space Research*, *27*(6–7), 1171–1179.

Walterscheid, R. L. (1981). Dynamical cooling induced by dissipating internal gravity waves. *Geophysical Research Letters*, *8*(12), 1235–1238.

Walterscheid, R. L., Hecht, J. H., Vincent, R. A., Reid, I. M., Woithe, J., & Hickey, M. P. (1999). Analysis and interpretation of airglow and radar observations of quasi-monochromatic gravity waves in the upper mesosphere and lower thermosphere over Adelaide, Australia (35°S, 138°E). *Journal of Atmospheric and Solar: Terrestrial Physics*, *61*, 461.

Walterscheid, R. L., Hecht, J. H., Djuth, F. T., & Tepley, C. A. (2000). Evidence of reflection of a long-period gravity wave in observations of the nightglow over Arecibo on May 8–9, 1989. *Journal of Geophysical Research*, *105*, 6927–6934.

Walterscheid, R. L., Schubert, G., & Brinkman, D. G. (2001). Small-scale gravity waves in the upper mesosphere and lower thermosphere generated by deep tropical convection. *Journal of Geophysical Research*, *106*(D23), 31,825–31,832. https://doi.org/10.1029/2000JD000131

Walterscheid, R. L., Hecht, J. H., Gelinas, L. J., Hickey, M. P., & Reid, I. M. (2012). An intense traveling airglow front in the upper mesosphere–lower thermosphere with characteristics of a bore observed over Alice Springs, Australia, during a strong 2 day wave episode. *Journal of Geophysical Research*, *117*, D22105. https://doi.org/10.1029/2012JD017847

Yuan, T., Pautet, P.-D., Zhao, Y., Cai, X., Taylor, M. J., & Pendleton, W. R. Jr. (2014). Coordinated investigation of mid-latitude upper mesospheric temperature inversion layers and the associated gravity wave forcing by Na lidar and Advanced Mesospheric Temperature Mapper in Logan, Utah. *Journal of Geophysical Research: Atmospheres*, *119*, 3756–3769. https://doi.org/10.1002/2013JD020586

Yue, J., She, C.-Y., Nakamura, T., Harrell, S., & Yuan, T. (2010). Mesospheric bore formation from large-scale gravity wave perturbations observed by collocated all-sky OH imager and sodium lidar. *Journal of Atmospheric and Solar: Terrestrial Physics*, *72*, 7–18.

Zhao, Y., Taylor, M. J., & Chu, X. (2005). Comparison of simultaneous Na lidar and mesospheric nightglow temperature measurements and the effects of tides on the emission layer heights. *Journal of Geophysical Research*, *110*, D09S07. https://doi.org/10.1029/2004JD005115

Zhao, Y., Taylor, M. J., Liu, H.-L., & Roble, R. G. (2007). Seasonal oscillations in mesospheric temperatures at low-latitudes. *Journal of Atmospheric and Solar: Terrestrial Physics*, *69*, 2367–2378.